# The Martian ionosphere at solar minimum: Empirical model validation using MAVEN ROSE data

Sophie R. Phillips [a], Clara Narvaez [a,*], František Němec [b], Paul Withers [a], Marianna Felici [a], Michael Mendillo [a]

[a] Center for Space Physics, Boston University, Boston, MA 02215, United States of America
[b] Faculty of Mathematics and Physics, Charles University, Prague, Czech Republic

## ARTICLE INFO

## ABSTRACT

The Radio Occultation Science Experiment (ROSE; Withers et al., 2018, 2020) on the Mars Atmosphere and Volatile EvolutioN (MAVEN) satellite has produced over 400 electron density profiles from July 2016 to November 2019. These $N_e(h)$ profiles occurred over a large range of solar zenith angles (54°- 130°) and solar flux conditions (24–54 solar flux units at Mars). One of the goals of the MAVEN mission is to characterize the status of the topside ionosphere at Mars as a reservoir of possible escaping plasma. Here we evaluate how ROSE topside ionospheric measurements, made predominantly under solar minimum conditions, compare with the only empirical model of the topside ionosphere (Němec et al., 2019). To assess congruence between the model and the observations, a deviation factor (DF) is calculated for each predicted versus observed $N_e(h)$ profile. Diurnally, low DFs (and thus higher agreement) occur for occultations with solar zenith angles (SZA) < 82°. On a longer time scale, lower solar fluxes tend to have higher DF values. Correlations of the maximum electron density ($N_{max}$) of each profile (predicted and observed) have an overall correlation coefficient (CC) of 0.96. Similarly, the observed total electron content of the topside ionosphere (TTEC) agrees with predictions (CC = 0.86). The model and the predictions differ most for the altitude of peak density (CC = 0.62 for SZA < 90°).

## 1. Introduction

The Mars Atmosphere Volatile EvolutioN (MAVEN, Jakosky, 2015) mission provides an unprecedented opportunity for long-term studies of the Martian ionosphere. While MAVEN's in-situ instruments provide observations along slanted orbital paths, the Radio Occultation Science Experiment (ROSE, Withers et al., 2018, 2020) offers a closer approximation of vertical structure. ROSE uses line-of-sight (Earth-satellite) telemetry observations during a small orbit segment—together with assumptions of ionospheric spatial consistency over the occultation ray path geometry—to produce nearly vertical electron density profiles, $N_e(h)$, typically over a time span of ~8 min.

ROSE topside ionosphere measurements are ideal for comparisons to the empirical model developed by Němec et al. (2019) using the vertical electron density profiles measured by the Mars Advanced Radar for Subsurface and Ionosphere Sounding (MARSIS) on board the Mars Express (MEX) spacecraft (Gurnett et al., 2005; Morgan et al., 2013; Němec et al., 2016). This model uses five parameters to describe each electron density profile: peak electron density, peak altitude, profile steepness at high altitudes, main layer thickness, and the transition altitude beyond which transport starts to dominate. These parameters are calculated for given conditions using empirical formulas in the model parameterized by SZA, Sun-Mars distance, F10.7 index value, and crustal magnetic field magnitude at an altitude of 400 km (from Cain et al., 2003). For solar flux, the F10.7 radio flux measured at Earth is adjusted to the "rotated-sun" date, i.e., the date when the Mars-facing solar hemisphere faced Earth where the F10.7 flux is observed. Once the five parameters are determined, the model electron density profile above the peak altitude can be retrieved. We note that the model was derived using electron density profiles measured at SZAs lower than 80 degrees spanning from the peak altitude up to 325 km. Although the model can be technically used to calculate electron densities beyond these limits (as done here), the corresponding precision is expected to be significantly lower.

---

* Corresponding author.
  *E-mail address:* cnarvaez@bu.edu (C. Narvaez).

## 2. Method

There is no "standard way" to compare electron density profiles obtained by observations with predictions from numerical models. At Earth, the International Reference Ionosphere (IRI) has a long history of development and validation (http://irimodel.org/). Each use of IRI has a particular data set for comparisons. For example, it can be used to predict vertical $N_e(h)$ patterns at fixed locations (as in Mendillo and Wroten, 2019), or a sequence of $N_e$ versus height predictions along a satellite orbit. The same situation occurs at Mars. While comparisons of predicted and observed electron density values can be made at each height, there is no accepted protocol for assessing entire profiles. There are, of course, many ways one might do that, and we urge the community to consider a discussion of possibilities. Here, we developed an algorithm to produce a *single parameter* to characterize the agreement (or disagreement) of the model's prediction of an overall electron density profile. We name this the Deviation Factor (DF), defined as

$$DF = \left( \frac{\sqrt{\sum (\Delta_i)^2}}{n} \div N_{max} \right) \times 100 \tag{1}$$

with $\Delta_i = [N_e \text{ (predicted)} - N_e \text{ (observed)}]$ and $n$ equal to the total number of heights with data for each profile. Note that weighting the differences by the $N_{max}$ value provided by the model results in numerically small DF magnitudes, but nevertheless a consistent way to conduct such a study. With $N_{max}$ values higher at noon vs. near-terminator conditions, DF values are expected to be lower for smaller SZAs. Note, in particular, that DF values are not in percentages.

## 3. Data

This investigation uses 367 radio occultations profiles with SZA < $100^o$ obtained over a three-year period (5 July 2016–1 November 2019). The distribution of occultations by year is listed in Table 1. Each year is noted by a different colour to enable comparisons between the three years of low solar activity (2017-18-19) with the earlier year of higher solar flux (2016). In most cases, the ROSE profiles used had good coverage from below the height of maximum electron density ($h_{max} \sim$ 135 km) to 600 km.

During the time ROSE took these measurements, the solar cycle was in a declining phase. The solar radio flux index (F10.7) at Earth ranged from 108 to 67 flux units — corresponding to 54–24 units at 1.524 AU. While occultations occurred over a vast range of latitudes and longitudes, only 31 cases occurred where the crustal magnetic field values were above 20 nT.

## 4. Examples of observed and predicted $N_e(h)$ profiles and their DF values

ROSE $N_e(h)$ profiles can be obtained over a height range that often exceeds the physical span of the ionosphere. In figures below, we will show ROSE data to 600 km altitude in order to portray the transition from relative smooth patterns below ~300 km to the more chaotic signatures at higher altitudes. Many of these top-side signatures have strong negative gradients that may well be indications of the "ionopause" at Mars (see review in Sánchez-Cano et al., 2020). The empirical model of Nĕmec et al. (2019) does not deal with possible ionopause effects for obvious reasons—it is a climatological model, not a real-time prediction scheme.

Fig. 1 shows a case we consider to include an ionopause effect near 300 km, with the model offering good agreement at altitudes below 300 km (the DF = 0.09). Fig. 2 offers additional examples of data-model comparison over a larger range of altitudes and higher solar zenith angles, with DF values of 0.10 and 0.18, respectively. Note that the altitude resolution is greater near $h_{max}$ and thus DF values have a higher contribution from data near the peak.
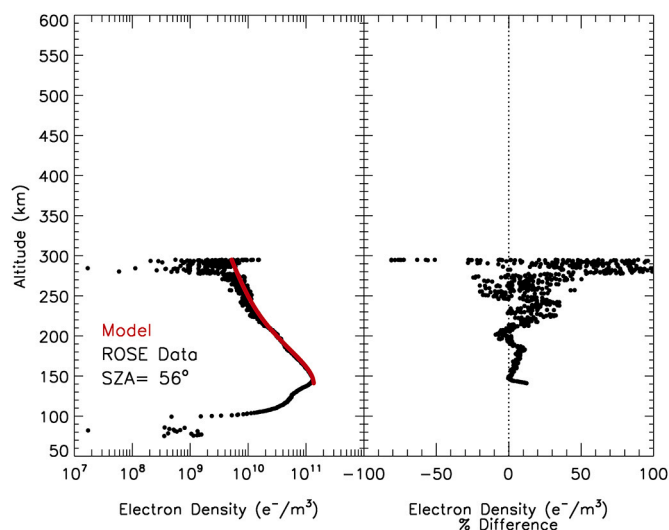


**Fig. 1.** Radio Occultation for October 8, 2016, which had a Deviation Factor of 0.09. Left panel shows model in red and ROSE measurements as black points. Right panel shows difference (model – data) in percent. Note that the right panel only shows values out to 100% for display purposes; higher values do exist and contribute to the deviation factor calculations. (For interpretation of the references to colour in this figure legend, the reader is referred to the web version of this article.)

**Table 1**
Number of ROSE occultations per year.

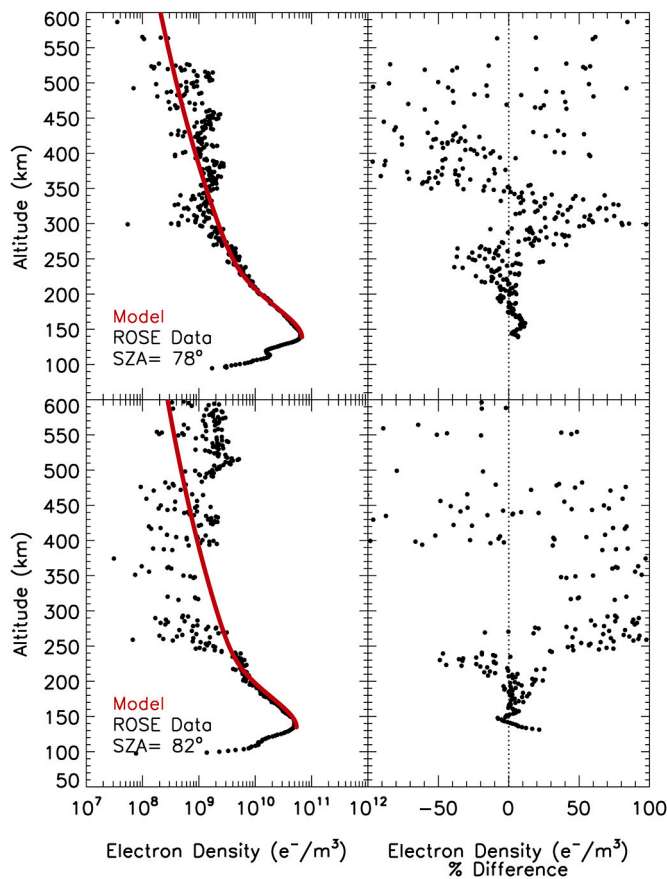| Year | SZA < $90^o$ | $90^o \leq SZA < 100^o$ | # of occultations | Average Solar Flux at 1AU |
|---|---|---|---|---|
| 2016 | 20 | 4 | 24 | 90.4 |
| 2017 | 37 | 22 | 59 | 76.7 |
| 2018 | 65 | 70 | 135 | 72.0 |
| 2019 | 97 | 52 | 149 | 72.1 |
| Total | 219 | 148 | 367 | 77.8 |

**Fig. 2.** Same format as in Fig. 1. (Top) Radio Occultation for 23 March 2018 having a Deviation Factor of 0.10. (Bottom) Radio Occultation for 13 July 2019 having a Deviation Factor of 0.18.

Fig. 3 shows examples of poor agreement (higher DF values) for post-terminator conditions characterized by SZA = 99°.

## 5. Additional analyses: maximum electron density and topside electron content

For more insight into how well the model matches ROSE data, we conducted an analysis of the measured and model values of maximum electron density ($N_{max}$). The results for each year are shown in Fig. 4, together with their linear correlation coefficients (CC). The solar cycle declining phase years (2016–2018) are comparable, while the deep solar minimum year (2019) shows more variability (i.e., lowest CC value).

We conducted the same analysis for the Total Electron Content of the topside ionosphere—calculated by integrating each electron density profile between $h_{max}$ and 400 km. We call this the Topside TEC (TTEC), using the same units as with full TEC ($10^{11}$ e$^-$/cm$^2$). The results are shown in Fig. 5 for each year. Again, the deep solar minimum year (2019) has more variability (lowest CC value) between model and observations than seen for earlier years.

The TTEC correlations, while high, are not as strong as those observed for $N_{max}$. Perhaps this can be explained by differences in the heights of peak density, which would affect the range of integration. To explore this, we show in Fig. 6 the lack of good agreement between ROSE observations and Model predictions of $h_{max}$. The solid black line shows the correlation of the entire data set used, while the correlations for individual years are shown in the legend. The dashed line represents heights where the modeled and measured peak heights are the same. It is worth noting that many values lie on or close to this line, but the overall correlation is affected by several points with very high or very low peak heights.
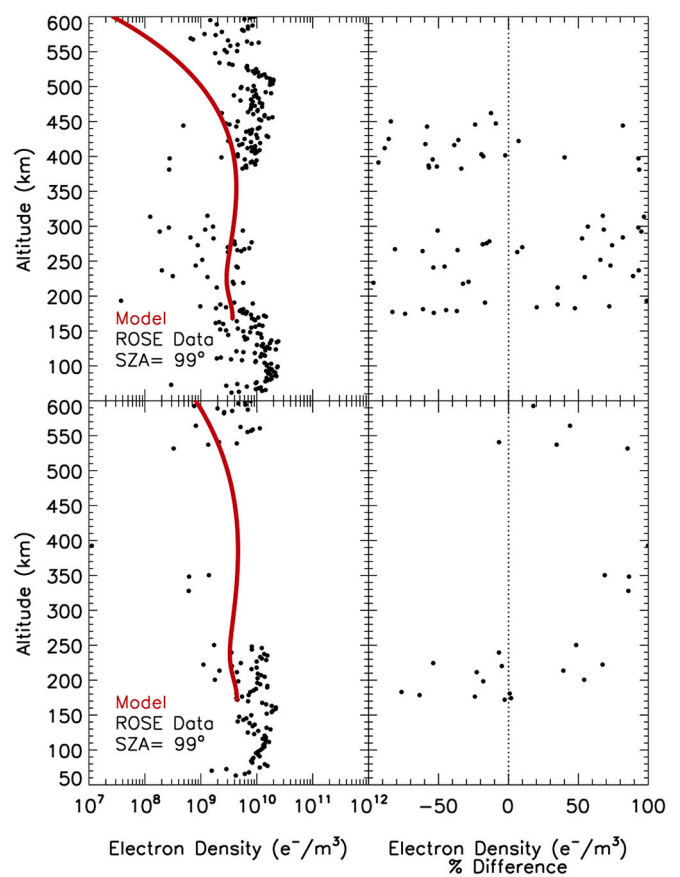


**Fig. 3.** Same format as in Figs. 1 and 2. (Top) Radio Occultation for 26 May 2019 with a Deviation Factor of 12. (Bottom) Radio Occultation for 10 February 2019 with a Deviation Factor of 15.8. Data gaps (e.g., between 400 and 500 km in lower panel) occur when the ROSE data-retrievals yield negative numbers for electron density. (For interpretation of the references to colour in this figure legend, the reader is referred to the web version of this article.)
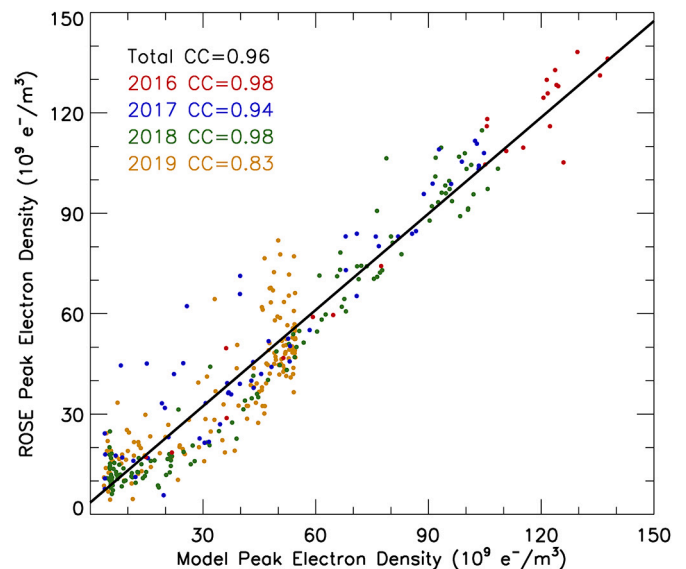


**Fig. 4.** Comparison of Model peak electron density and ROSE peak electron density for each year's occultations. Colour coding is as defined in Table 1. (For interpretation of the references to colour in this figure legend, the reader is referred to the web version of this article.)
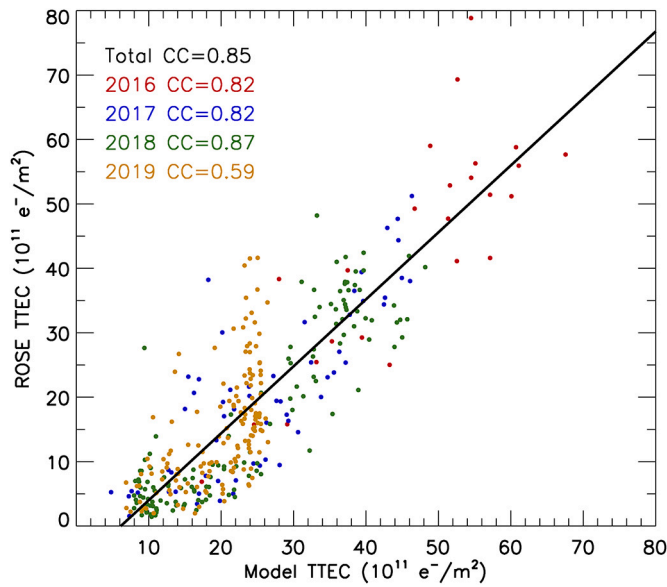
**Fig. 5.** Comparison of topside total electron content (TTEC) values (model vs observations) for each year's occultations.
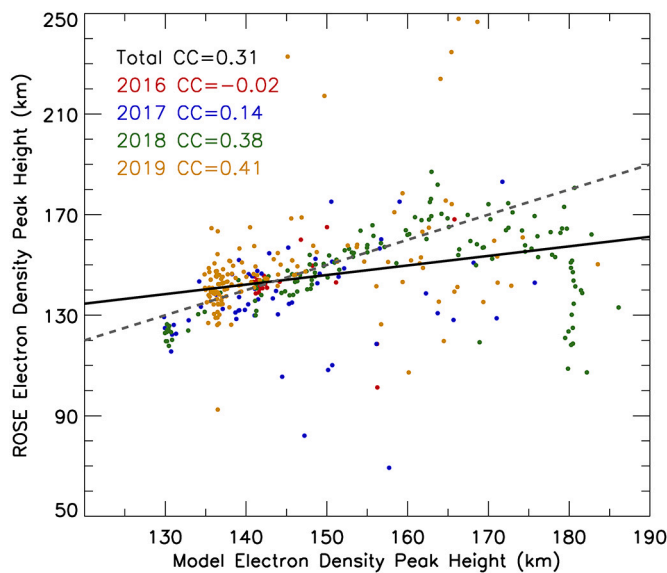


**Fig. 6.** Comparison of the heights of maximum electron densities from ROSE observations and the model (Němec et al., 2019). The same colour coding used in Figs. 4 and 5 specifies annual data sets. The dashed line indicates the trend for perfect model-data agreement. (For interpretation of the references to colour in this figure legend, the reader is referred to the web version of this article.)

## 6. Analyses of DF values: occurrence, SZA and crustal-B patterns

Fig. 7 shows a histogram portraying the distribution of DF values that range from 0.08–16. We find no dependence of DF values on the Mars-Sun distance. A strong majority of values fall in the lowest bin (DF = 0–2), meaning that the model does an excellent job in predicting the $N_e(h)$ topside ionosphere profiles observed by MAVEN's radio occultation science experiment. The highest DF values (12 and 16) are those shown in Fig. 3 for conditions of large SZAs (99°).

The full dependence of the DF values on SZA conditions is portrayed in Fig. 8. Each year is plotted using the same colour coding as in earlier figures, and the average DF values for every 10° of SZA are shown using black dots with associated uncertainty bars. Clearly, the DF values
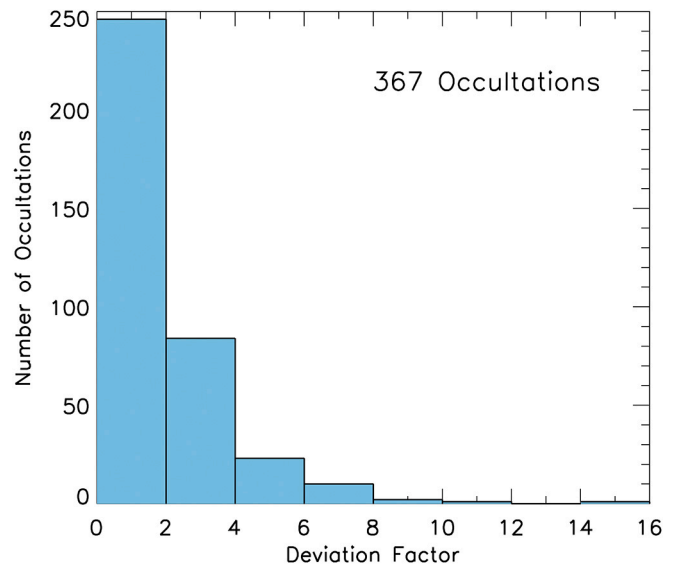


**Fig. 7.** Histogram showing DF occurrence frequency for every 2 units.
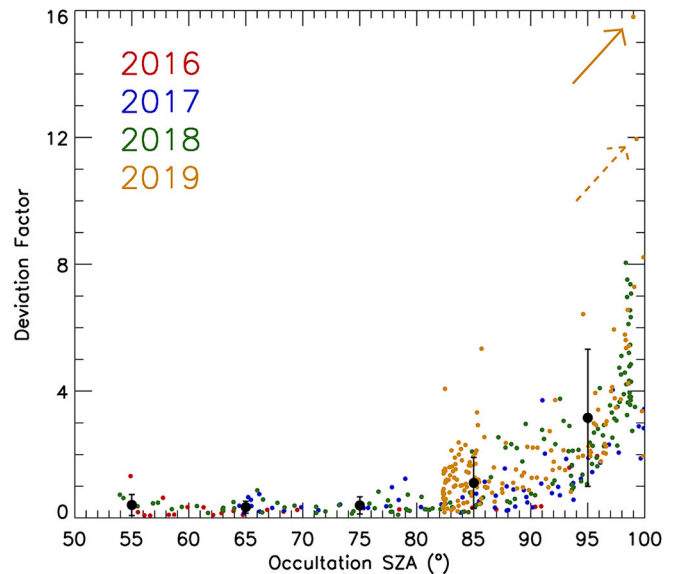


**Fig. 8.** Deviation Factor vs SZA for each occultation. The dashed and solid arrows indicate the occultations shown in Fig. 3 (top/bottom, respectively). Average DF values (black dots) with uncertainty bars are plotted for each 10° interval.

increase and have a higher variability as the SZA increases. This arises, in part, from the fact that at high SZAs the $N_{max}$ is lower and thus the metric of model performance (Eq. (1))—normalization by $N_{max}$—will increase DFs at higher SZAs.

While less than 10% of the ROSE occultations occurred in regions of crustal B-fields greater than 20 nT, it is worthwhile examining DF patterns in such areas. Recall that the model takes the B-field magnitude at 400 km (Cain et al., 2003) into account in making its predictions (Němec et al., 2019). Fig. 9 summarizes the relationship between Deviation Factors and crustal-B magnitudes. There is no statistically-significant trend in these results.

## 7. Solar cycle effects

To investigate the effects of long-term solar activity upon the Martian ionosphere—as observed by MAVEN/ROSE and the empirical
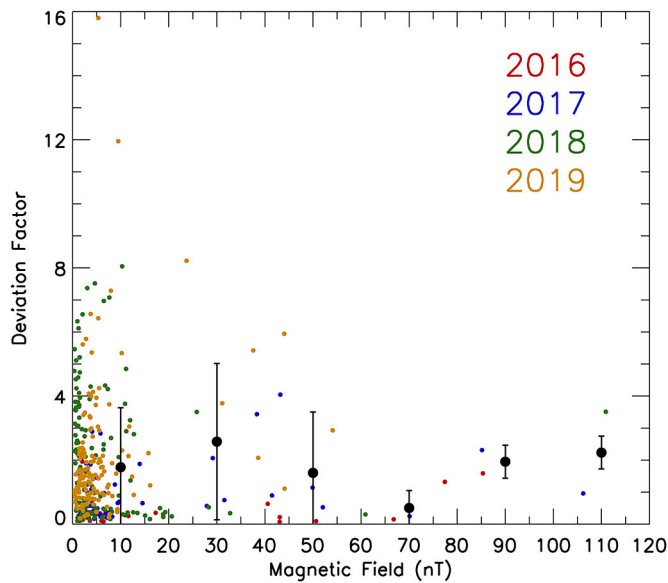
**Fig. 9.** Deviation Factor of each occultation vs its respective magnetic field value. Average DF values with uncertainty bars for each 20 nT interval are plotted as black dots and bars.

model used to represent it (Němec et al., 2019)—we examined two characterizations of solar input. First, we used the solar input required by the model, the solar radio flux at 10.7 cm, adjusted to its date of observation at Earth with respect to observations at Mars—the so-called "rotated-Sun" method (e.g., Mendillo et al., 2016). Prior to the MAVEN mission, this had long been the proxy index for solar flux that could be used at Mars (adjusted for $1/d^2$ effects). The second method now available is to use the daily solar irradiance observations made by the EUV instrument on MAVEN (Eparvier et al., 2015). Summing over the wavelength bins most responsible for ionization of $CO_2$ (0.1–93 nm) for each day of an occultation, the irradiance pattern can be compared to DF values. The results using both methods are shown in Fig. 10, with F10.7 correlations in the top panel and the EUV correlations below.

There is a clear trend in Fig. 10 with lower flux values having higher DF values. This is an unanticipated result—the ionosphere is more variable and thus less-well predicted by a climatological model during solar minimum years. This pattern is also apparent in the results shown in Fig. 4. We note in this context that the empirical model was derived using data from the MARSIS radar on Mars Express between Aug 2005 and Oct 2015, and the ROSE observations are from 2016 to 2019. Both data sets thus include the declining phase of a solar cycle.

## 8. Comparative studies of ionospheric variability

This study dealt with the topside ionosphere of Mars—from the height of maximum electron density ($h_{max}$ near 130–140 km) up to altitudes of 600 km. The top height is beyond the planet's "ionopause" that is typically below 400 km (Sánchez-Cano et al., 2020). Yet, there is a continuity of the ROSE $N_e(h)$ values (with increased variability) suitable for comparison with an empirical model (Němec et al., 2019) that covers the same altitude range. The plasma conditions at $h_{max}$ are strongly controlled by photo-chemical-equilibrium (PCE) processes, while above heights of ~170 km the time-constants for plasma chemistry and dynamics are comparable (see Fig. 16 in Mendillo et al., 2011), and thus multiple processes contribute to $N_e(h)$ profiles. At $N_{max}$, we found excellent agreement between model predictions and ROSE observations (Fig. 4). For the integrated electron content of the topside ionosphere, we found a lower (though acceptable) correlation between model and data (Fig. 5). The latter is consistent with the increasing role of variable
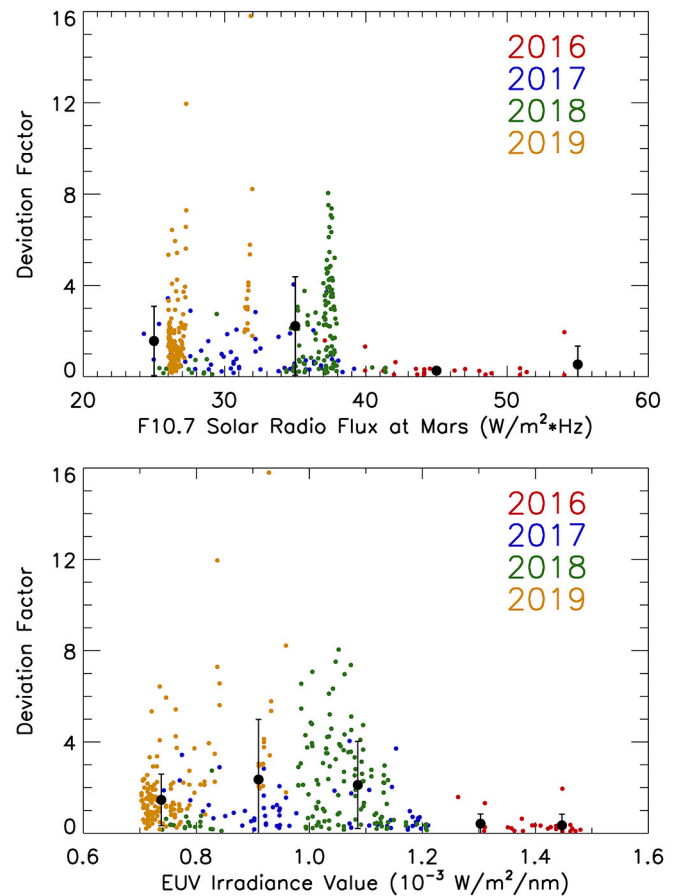




**Fig. 10.** Deviation Factor of each occultation vs its respective F10.7 solar radio flux and solar EUV irradiance value. Average DF values with uncertainty bars for each 10 solar flux unit intervals (top) and for 0.2 EUV irradiance intervals (bottom) are plotted as black dots. The F10.7 values are for the rotated-Sun dates, while the EUV irradiance values are for observations made at Mars on the days of ROSE occultation data. (For interpretation of the references to colour in this figure legend, the reader is referred to the web version of this article.)

plasma transport in the topside ionosphere.

In the Earth's ionosphere, the maximum electron density occurs in the F-layer where both photo-chemistry and plasma dynamics occur. Ionospheric variability studies at Earth typically deal with the standard deviation (in percent) about monthly mean values. For the F-layer, this results in $\sigma = 20–25\%$ for all local times, seasons and solar cycle conditions (Rishbeth and Mendillo, 2001; Mendillo, 2020). For Earth-Mars comparisons, the terrestrial layers dominated by photo-chemical-equilibrium (PCE) must be used. These are the *E*-region near 110 km and the F1 layer at ~170 km. For the E-region, variability at mid-day is typically 7–12% (Moore et al., 2006). The F1-layer is highly correlated with the E-layer (Mendillo et al., 2016), and thus exhibits comparable variability. To explore the sources of E-layer variability, Moore et al. (2006) showed that the contribution to variability from solar input (changes in flux and declination over a month) was 8–9%. The remaining contributions came from small changes in the neutral atmosphere.

To see if the terrestrial E-region has a variability that changes over the course of a solar cycle, we examined long-term observations from a mid-latitude station (Chilton, UK). Fig. 11 shows diurnal patterns of the maximum electron density of the E-layer ($N_mE$) during years of solar minimum (left and right panels) and the intervening year of solar maximum. A visual comparison shows that this terrestrial PCE layer has minimal changes of variability spanning a solar cycle. Quantitatively,
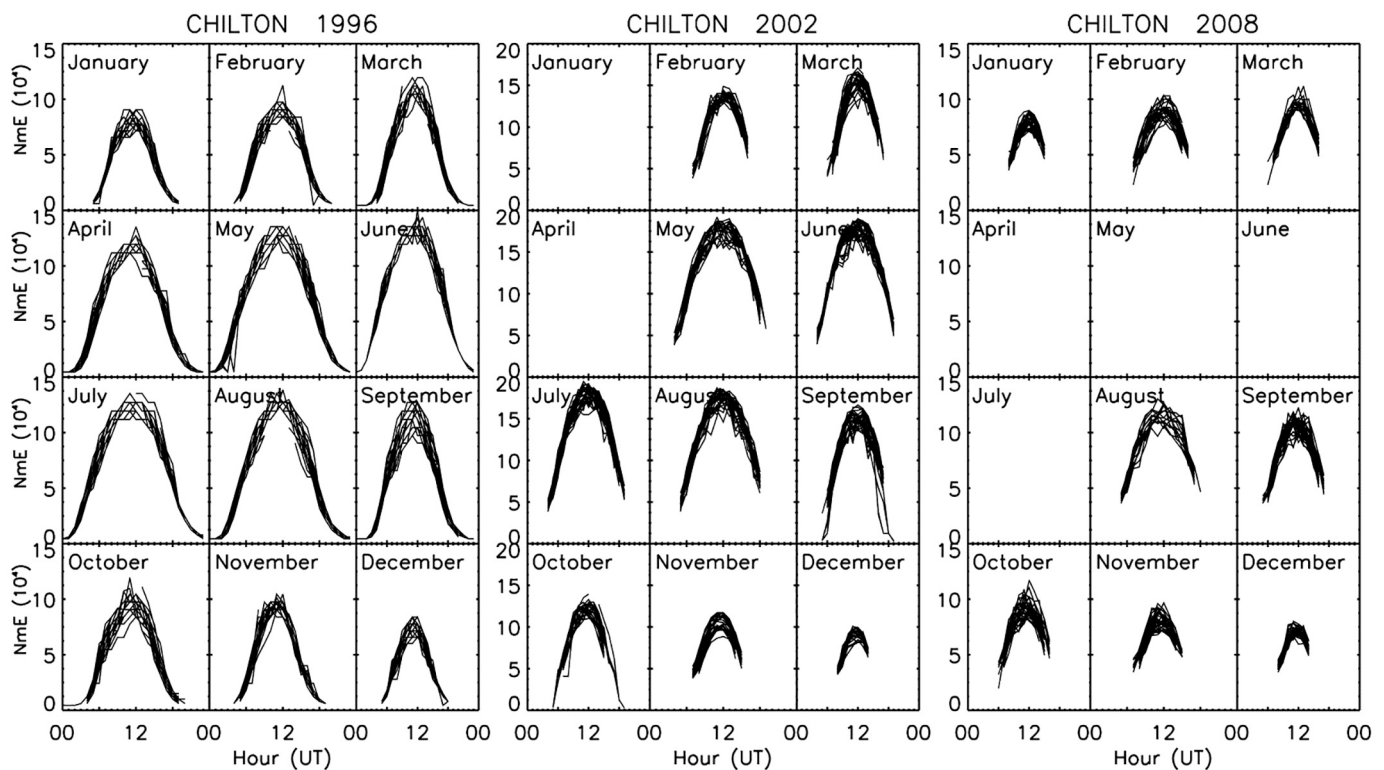
**Fig. 11.** Ionosonde measurements of the hourly values of the peak electron density of the *E*-layer at a mid-latitude station (Chilton, UK) during years of low solar flux (left, 1996; right, 2008) in comparison to a year of high solar flux (2002). Some months have no observations due to equipment failures.

the variability falls between 5 and 9% for all months during each phase of the solar cycle. This is separate from the trend of lower absolute values of $N_mE$ from solar max to solar min (2002–2008) due to photon irradiance changes. Our preliminary conclusion is that ionospheric variability at Mars during periods of low solar flux exceeds that at Earth. While this inference comes from ionospheric layers in the PCE-dominated height ranges (Figs. 4 and 11), such trends set the base values for transitions into the topside ionospheres where plasma transport occurs.

## 9. Discussion

We have used a new data source of ionospheric electron density profiles at Mars – obtained by MAVEN's Radio Occultation Science Experiment (ROSE) described in Withers et al. (2018, 2020)— to test the accuracy of an empirical model of the Martian topside ionosphere developed using radar observations from Mars Express (Němec et al., 2019). To characterize an observed profile's overall agreement (or disagreement) with model predictions, a Deviation Factor (DF) index was defined for use. A majority of the comparisons had low DF values, indicating that the model accurately predicts electron density profiles in the topside ionosphere. Model accuracy decreased at SZAs above 80°, as anticipated for the highly variable and structured profiles often observed near the solar terminators (dawn and dusk), as well as the fact that the model was developed using data with SZA less than 80 degrees. No significant trend for DF values occurred near or far from regions with crustal magnetic fields. Comparisons of ROSE peak density and the topside ionosphere's Total Electron Content—two key characteristics of an electron density profile—revealed a high agreement between model and measurements.

There are, nevertheless, issues that remain for future studies. These include possible observational biases in the contributions to the Deviation Factor from different altitude regimes in the topside ionosphere. The current empirical model (Němec et al., 2019) also used the Earth-based solar parameter F10.7 in conjunction with Mars Express data. With solar EUV now available from MAVEN, a more direct linkage between solar production and observed electron densities is now possible for next generation empirical modeling. Representation of the magnetic field used in the empirical model (Němec et al., 2019), while not a major source of variability in our DF analyses, can also be upgraded to a more recent MAVEN-based model (e.g., Langlais et al., 2019).

Finally, the un-anticipated result was that during a year of deep solar minimum activity (2019) ionospheric variability at Mars was higher than found during a year of higher activity (2016). This trend is not found for the terrestrial *E*-layer, a region under similar photo-chemical-equilibrium control. Future comparative studies—observational and modeling—need to address how neutral atmosphere seasonal patterns and omni present wave activity at Mars might contribute to higher ionospheric variability during periods of low solar activity.

## Declaration of Competing Interest

None

## Acknowledgements

WG/Observatory/GIRO

## References

Cain, J.C., Ferguson, B.B., Mozzoni, D., 2003. An $n = 90$ internal potential function of the Martian crustal magnetic field. J. Geophys. Res. 108 (E2), 5008. https://doi.org/10.1029/2000JE001487.

Eparvier, F.G., Chamberlin, P.C., Woods, T.N., Thiemann, E.M.B., 2015. The solar extreme ultraviolet monitor for MAVEN. Space Sci. Rev. 195, 293–301. https://doi.org/10.1007/s11214-015-0195-2.

Gurnett, D.A., Kirchner, D.L., Huff, R.L., Morgan, D.D., Persoon, A.M., Averkamp, T.F., et al., 2005. Radar soundings of the ionosphere of Mars. Science 310, 1929–1933. https://doi.org/10.1126/science.1121868.

Jakosky, B., 2015. MAVEN explores the martian upper atmosphere. Science 350 (6261), 643. https://doi.org/10.1126/science.aad3443.

Langlais, B., Thébault, E., Houliez, A., Purucker, M.E., Lillis, R.J., 2019. A new model of the crustal magnetic field of Mars using MGS and MAVEN. J. Geophys. Res. Planet 124, 1542–1569. https://doi.org/10.1029/2018JE005854.

Mendillo, M., 2020. Day-to-day variability of the ionosphere. In: Materassi, M., Forte, B., Coster, A.J., Skone, S. (Eds.), The Dynamical Ionosphere—A Systems Approach to Ionospheric Irregularity. Elsevier, Amsterdam.

Mendillo, M., Wroten, J., 2019. Modeling stable auroral red (SAR) arcs at geomagnetic conjugate points: implications for hemispheric asymmetries in heat fluxes. J. Geophys. Res. Space Physics 124, 6330–6342. https://doi.org/10.1029/2019JA026904.

Mendillo, M., Lollo, A., Withers, P., Matta, M., Patzold, M., Tellmann, S., 2011. Modeling Mars' ionosphere with constraints from same-day observations by Mars Global Surveyor and Mars Express. J. Geophys. Res. Space Physics 116, A11303. https://doi.org/10.1029/2011JA016865.

Mendillo, M., Trovato, J., Narvaez, C., Mayyasi, M., Moore, L., Vogt, M.F., Fallows, K., Withers, P., Martinis, C., 2016. Comparative aeronomy: molecular ionospheres at Earth and Mars. J. Geophys. Res. Space Physics 121 (10), 269–10,288. https://doi.org/10.1002/2016JA023097.

Moore, L., Mendillo, M., Martinis, C., Bailey, S., 2006. Day-to-day variability of the $E$ layer. J. Geophys. Res. 111, A06307 https://doi.org/10.1029/2005JA011448.

Morgan, D.D., Witasse, O., Nielsen, E., Gurnett, D.A., Duru, F., Kirchner, D.L., 2013. The processing of electron density profiles from the Mars express MARSIS topside sounder. Radio Sci. 48, 197–207. https://doi.org/10.1002/rds.20023.

Němec, F., Morgan, D.D., Gurnett, D.A., 2016. On improving the accuracy of electron density profiles obtained at high altitudes by the ionospheric sounder on the Mars express spacecraft. J. Geophys. Res. Space Physics 121, 10,117–10,129. https://doi.org/10.1002/2016JA023054.

Němec, F., Morgan, D.D., Kopf, A.J., Gurnett, D.A., Pitoňák, D., Fowler, C.M., 2019. Characterizing average electron densities in the Martian dayside upper ionosphere. J. Geophys. Res. Planet 124, 76–93. https://doi.org/10.1029/2018JE005849.

Reinisch, B.W., Galkin, I.A., 2011. Global ionospheric radio observatory (GIRO). Earth Planet Space 63, 377–381. https://doi.org/10.5047/eps.2011.03.001.

Rishbeth, H., Mendillo, M., 2001. Patterns of ionospheric variability. J. Atmos. Solar Terr. Phys. 63, 1661–1680.

Sánchez-Cano, B., Narvaez, C., Lester, M., Mendillo, M., Mayyasi, M., Holmstrom, M., et al., 2020. Mars' ionopause: a matter of pressures. J. Geophys. Res. Space Physics 125. https://doi.org/10.1029/2020JA028145 e2020JA028145.

Withers, P., Felici, M., Mendillo, M., Moore, L., Narvaez, C., Vogt, M.F., Jakosky, B.M., 2018. First ionospheric results from the MAVEN radio occultation science experiment (ROSE). J. Geophys. Res. Space Physics 123, 4171–4180. https://doi.org/10.1029/2018JA025182.

Withers, P., Felici, M., Mendillo, M., et al., 2020. The MAVEN radio occultation science experiment (ROSE). Space Sci. Rev. 216, 61. https://doi.org/10.1007/s11214-020-00687-6.